



# Protonic acid-assisted universal synthesis of defect abundant multifunction carbon nitride semiconductor for highly-efficient visible light photocatalytic applications



Shipeng Wan<sup>a,b</sup>, Man Ou<sup>a</sup>, Yanan Wang<sup>a,e</sup>, Yiqing Zeng<sup>a,e</sup>, Yongheng Xiong<sup>a,e</sup>, Fujiao Song<sup>c</sup>, Jie Ding<sup>a,e</sup>, Wei Cai<sup>d</sup>, Shule Zhang<sup>a,e</sup>, Qin Zhong<sup>a,e,\*</sup>

<sup>a</sup> School of Chemical Engineering, Nanjing University of Science and Technology, Nanjing, Jiangsu, 210094, PR China

<sup>b</sup> School of Chemical & Biomedical Engineering, Nanyang Technological University, 62 Nanyang Drive, 637459, Singapore

<sup>c</sup> School of Environmental Science and Engineering, Yancheng Institute of Technology, Yancheng, 224000, PR China

<sup>d</sup> School of Environmental Science and Engineering, Nanjing University of Information Science and Technology, Nanjing, 210044, PR China

<sup>e</sup> Nanjing AIREP Environmental Protection Technology Co., Ltd, Nanjing, Jiangsu, 210091, PR China

## ARTICLE INFO

### Keywords:

Hexagonal tubular carbon nitride  
Defects  
Highly-efficient  
Multifunction photocatalytic applications  
Visible light

## ABSTRACT

To circumvent the low charge transportation efficiency, poor photocatalytic activity and selectivity of carbon nitride semiconductor, and achieve multifunction photocatalytic applications, the hexagonal tubular carbon nitride with abundant useful nitrogen defects and oxygen-containing defects have been successfully fabricated via supramolecular hydrogen-bonded self-assembly hydrothermal strategy. The resultant hexagonal tubular carbon nitride exhibits highly-efficient photocatalytic H<sub>2</sub> evolution rate of 7.95 mmol·g<sup>-1</sup> h<sup>-1</sup> and photocatalytic CO<sub>2</sub> conversion to CO with 92.4% selectivity, much better than that of most previously reported carbon nitride base photocatalysts. Moreover, the hexagonal tubular carbon nitride also achieves remarkable visible light photocatalytic NO removal efficiency of 81.97%, increasing by 65.95% than that of g-CN. This systematic and substantial work convincingly proved that the hexagonal tubular carbon nitride with abundant defects could be easily achieved by this approach, and provided a feasible strategy for highly-efficient photocatalytic H<sub>2</sub> evolution, CO<sub>2</sub> reduction and NO removal under visible light, simultaneously.

## 1. Introduction

The excessive consumption of fossil resources, especially for coal resource combustion accompanied by the massive emission of flue gas containing carbon dioxide and nitrogen oxide (3–15% CO<sub>2</sub> and 100–500 ppm NO<sub>x</sub> containing 95% NO) has resulted in the urgent demand for sustainable clean energy alternative to fossil fuels, and controlling the emission of gas pollutants [1–3]. Therefore, different strategies, including photocatalysis, thermocatalysis and electrocatalysis, have been developed to resolve these problems [4–11]. Wherein photocatalytic technology utilizing inexhaustible solar energy as energy source could be regarded as a promising strategy to ameliorate the energy and environment issues in the future [12–15]. Amounts of semiconductor materials have been designed and fabricated for photocatalytic application, such as water splitting to H<sub>2</sub>, CO<sub>2</sub> reduction, pollutant degradation and organic photocatalysis [16–22]. Among them, graphitic carbon nitride (g-CN) has attracted tremendous

attention in photocatalytic fields due to its excellent thermal and chemical stability, and appealing electronic structure [23–25]. However, the low photocatalytic activity significantly restricts its scale application, originating from the poor visible light absorption capacity, low specific surface area and charge transportation efficiency. Various efficient strategies have been developed to circumvent these obstacles, such as nanostructure design with templates, doping with metal and non-metal, surface treatment by alkali or acid, forming heterojunction with other semiconductors [26–31]. Note that each of these methods exists the inherent drawback. For example, the templating-method for nanostructure design is commonly used to achieve carbon nitride nanotube or nanosphere with enhanced photocatalytic performance, but this approach involves the removal of templates (e.g., silicon dioxide, anodic aluminum oxide, surfactants, ionic liquids), which is time-consuming and inefficient, and affects the functionalization of material surface [26,32]. As well, the one-dimensional (1D) tubular structures has also aroused great attention in the oriented transfer of charge

\* Corresponding author at: School of Chemical Engineering, Nanjing University of Science and Technology, Nanjing, Jiangsu, 210094, PR China.  
E-mail address: [zq304@njust.edu.cn](mailto:zq304@njust.edu.cn) (Q. Zhong).

carriers [33]. For instance, Grimes group has fabricated 1D tubular  $\text{TiO}_2$  with superior charge-carrier separation and transfer capacity in dye-sensitized solar cells [34]. Therefore, it is highly expected to develop other novel and feasible strategy to fabricate unique structure carbon nitride with highly-efficient photocatalytic performance.

Beyond that, defect engineering on the periodic tri-s-triazine frameworks becomes another prevailing approach to upgrade the photocatalytic performance of carbon nitride, and the structure termination anchoring cyano groups ( $\text{C}\equiv\text{N}$ ), amino groups ( $-\text{NH}_2$ ) as well as forming nitrogen vacancies was shown to be profitable for photocatalytic applications [35–37]. However, the carbon nitride accompanied by in situ formation of useful nitrogen defects and oxygen-containing defects on the surface still poses challenges as far as we know. Moreover, the oxidation and reduction properties of carbon nitride are rarely investigated simultaneously. Inspired by these findings, we still face the challenge and try our best to design a facile and feasible strategy to engineering abundant useful defects onto tubular carbon nitride for highly-efficient photocatalytic applications.

In this account, we successfully design a novel protonic acid (e.g.,  $\text{HNO}_3$ ,  $\text{H}_2\text{SO}_4$ ,  $\text{H}_3\text{PO}_4$ ) assisted hydrothermal route to fabricate a series of one-dimensional hexagonal tubular carbon nitrides via co-polymerization of melamine and cyanuric acid from in situ hydrolysis of melamine. Excitingly, the resultant hexagonal tubular carbon nitride possesses abundant nitrogen defects and oxygen-containing defect along with the increased specific surface area, enhanced visible light absorption capacity, improved redox ability, and enhanced photogenic electron separation ability, highlighting the versatility of the approach. More important, the hexagonal tubular carbon nitrides have achieved highly-efficient multifunction photocatalytic performance for  $\text{H}_2$  evolution,  $\text{CO}_2$  reduction and  $\text{NO}$  oxidation, simultaneously. Finally, the photocatalytic mechanism is proposed and discussed. The synthetic strategy adopted here thus provides a simple and effective route of synergistically optimizing the chemical composition, morphology structure, optical properties and charge transportation efficiency of carbon nitride base materials, and achieving highly-efficient photocatalytic applications.

## 2. Results and discussion

### 2.1. Structure and defect analysis

Initially, the XRD patterns of graphitic carbon nitride (g-CN) and the protonic acid induced carbon nitrides  $\text{CN}_{\text{Xt}}$  ( $\text{X}=\text{P}, \text{N}, \text{S}; t = 0.3, 0.6, 0.9, 1.2$ ) powders were first investigated (Fig. 1a and Fig. S3–S4). Two distinct characteristic peaks at  $13.3^\circ$  (100) and  $27.4^\circ$  (002) can be observed, corresponding to the in-plane packing of tri-s-triazine units parallel to c-axis and the periodic stacking of graphitic layers along the c-axis, respectively [38,39]. As compared to g-CN, the (002) peak become weaker and broader, suggesting the reduced crystal sizes [40]. The apparent disappearance of (100) peak originates from the damage of the ordered in-plane structure, which is assigned to the formation of nitrogen defects. As revealed by FTIR spectra (Fig. 1b and Fig. S5–S6),  $\text{CN}_{\text{Xt}}$  and g-CN exhibit the similar chemical structure. Wherein the peak at ca.  $808\text{ cm}^{-1}$  is related to the typical characteristic peak of tri-s-triazine unit. The peaks ranging from  $1200$  to  $1700\text{ cm}^{-1}$  belong to the stretching modes of aromatic heterocycles. The broad peaks between  $2900$  and  $3600\text{ cm}^{-1}$  corresponded to  $\text{N}-\text{H}$  and  $\text{O}-\text{H}$  stretching vibration. However, several differences for  $\text{CN}_{\text{Xt}}$  can be clearly observed in comparison with g-CN. An increased signal peak at  $1152\text{ cm}^{-1}$  corresponding to  $\text{C}-\text{O}$  stretching vibrations could be detected [38]. Although the  $\text{C}=\text{O}$  stretching vibrations of carboxyl group in  $\text{CN}_{\text{Xt}}$  are overlapped, a relatively stronger peak intensity at ca.  $1650\text{ cm}^{-1}$  can be observed [41–44]. A weak signal peak located at  $2168\text{ cm}^{-1}$  is assigned to the characteristic of cyano groups ( $\text{C}\equiv\text{N}$ ), which is derived from the deprotonation of  $-\text{C}-\text{NH}_2$  [45,46]. The increased intensities of the signal peaks corresponding to the  $\text{N}-\text{H}$  bond at ca.  $3168\text{ cm}^{-1}$  (violet

dotted box) and the  $\text{O}-\text{H}$  bond in carboxyl group at ca.  $3335\text{ cm}^{-1}$  (origin dotted box) originate from the loss of the in-plane periodicity of the tri-s-triazine framework, indicating the increase of defect numbers and active sites on the catalyst surface [38,42,47]. The chemical structure of CNPt, taking  $\text{CNP}_{0.6}$  and g-CN for an instance, has been further investigated by employing Solid-state  $^{13}\text{C}$  magic angle spinning NMR. As shown in Fig. 1c–d, both  $\text{CNP}_{0.6}$  and g-CN exhibits two distinct peaks at  $\delta_1$  (155.4 ppm) and  $\delta_2$  (163.2 ppm) corresponding to the chemical shifts of  $\text{C}_{3\text{N}}$  and  $\text{C}_{2\text{N}-\text{NH}_2}$  in the tri-s-triazine framework, respectively [48,49]. However, it's noteworthy that the new signal peaks at  $\delta_3$  (111.9 ppm) and  $\delta_4$  (124.9 ppm) for  $\text{CNP}_{0.6}$  can be observed, which is assigned to be the C atom in  $\text{C}\equiv\text{N}$  group, locating at the apex of the melon structure of carbon nitride [35]. And another new signals at  $\delta_5$  (178.5 ppm) and  $\delta_6$  (186.9 ppm) for  $\text{CNP}_{0.6}$  should be attributed to the neighbor C atom of  $\text{C}\equiv\text{N}$  group and the C atom in carboxyl group, respectively [42,50].

To further investigate the change of surface elemental composition and electronic structure of CNPt, XPS measurements were carried out (Fig. 1e–f and Fig. S7). The peaks at ca.  $288$ ,  $398$ ,  $532$  and  $134\text{ eV}$  in XPS survey spectra are respectively assigned to  $\text{C}\ 1\text{s}$ ,  $\text{N}\ 1\text{s}$ ,  $\text{O}\ 1\text{s}$  and  $\text{P}\ 2\text{p}$  signals (Fig. S7a). Note that the obviously increased O content for  $\text{CNP}_{0.6}$  could be detected in comparison with that of g-CN (Fig. S8a and Table S1). In the high resolution  $\text{C}\ 1\text{s}$  XPS spectra (Fig. 1e, right), the peaks at  $284.6$ ,  $285.8$  and  $288.2\text{ eV}$  are attributed to  $\text{sp}^2$ -hybridized carbon ( $\text{C}-\text{C}$ ) emanating from defective polymerization,  $\text{C}-\text{NH}_x$  on the edges of tri-s-triazine unit, and the  $\text{N}-\text{C}\equiv\text{N}$  coordination in the heterocycles, respectively [6]. As compared to g-CN (Fig. S8b), the signal peak at  $285.8\text{ eV}$  for  $\text{CNP}_{0.6}$  exhibits an increased intensity, which should be regarded as the additional evidence for the generation of  $\text{C}\equiv\text{N}$  group as confirmed by FTIR and solid-state  $^{13}\text{C}$  NMR, because the  $\text{C}\ 1\text{s}$  binding energy of  $\text{C}\equiv\text{N}$  group is similar to that of  $\text{C}-\text{NH}_x$  [51]. And a new peak at  $289\text{ eV}$  for  $\text{CNP}_{0.6}$  appears, suggesting the formation of  $\text{O}=\text{CO}$  bond [52–54]. Excitingly, the high-resolution  $\text{O}\ 1\text{s}$  XPS spectra further confirmed the existence of O-containing defects (Fig. 1f). An obvious signal peak at  $531.5\text{ eV}$  can be clearly observed, ascribing to  $\text{C}-\text{O}$  and  $\text{O}=\text{CO}$  species, the core level at  $532.6\text{ eV}$ , similar to g-CN, is assigned to the surface adsorbed water [38,41,55]. However, such signal species at  $531.5\text{ eV}$  is not detected for g-CN (Fig. S8d). Furthermore, it is worth mentioning that no signal peak corresponding to  $\text{N}-\text{O}$  at  $980\text{ cm}^{-1}$  has been detected as seen by FTIR spectra. The results indicate that the as-fabricated tri-s-triazine base CNPt possess the potential carboxyl oxygen-containing group. For the  $\text{N}\ 1\text{s}$  XPS spectra (Fig. 1e, left), four peaks at  $398.7$ ,  $399.4$ ,  $401.0$  and  $404.6\text{ eV}$  are attributed to two-coordinated N atoms in  $\text{C}-\text{N}=\text{C}$  group ( $\text{N}_{2\text{C}}$ ), three-coordinated N atoms in  $\text{N}-(\text{C})_3$  group ( $\text{N}_{3\text{C}}$ ),  $\text{NH}_x$ , and positive charge localization in the heterocycles ( $\text{C}-\text{N}-\text{H}$ ), respectively [56]. As summarized in Table S2, the N/C atomic ratios on the surface for g-CN were  $1.301$ , while the N/C atomic ratio for  $\text{CNP}_{0.6}$  were only  $1.005$ , smaller than that of g-CN. The decreased tendency indicated an increased N-vacancy concentration for  $\text{CNP}_{0.6}$ , which is consistent with the variation tendency of elemental analysis (Table S3). Moreover, the peak area ratio for  $\text{N}_{2\text{C}}$  and  $\text{N}_{3\text{C}}$  also exhibited a decreased tendency from  $3.399$  for g-CN to  $1.834$  for  $\text{CNP}_{0.6}$ , which evidently confirmed the formation of N vacancies on the surface of carbon nitride. The preferential missing of N species in  $\text{N}_{2\text{C}}$  originated from the unsaturated coordinations, which results in the redistribution of electrons among the aromatic  $\pi$ -conjugated system of carbon nitride, establishing new charge balance. Moreover, the results of EPR measurement further confirmed the relationship between unpaired-electron variation and N vacancy (Fig. S9). An ignorable Lorentzian line EPR signal for g-CN is occurred at a g value of  $2.0023$ , deriving from few unpaired electrons on C atoms of  $\pi$ -conjugated aromatic rings [57,58]. As compared to g-CN, a significantly enhanced spin intensity for  $\text{CNP}_{0.6}$  is detected due to the formation of high concentration N vacancy, increasing the number of unpaired electrons on C atoms of the aromatic heterocycles [59]. Similar results can be achieved from high-resolution  $\text{N}\ 1\text{s}$ ,  $\text{C}\ 1\text{s}$  and  $\text{O}\ 1\text{s}$

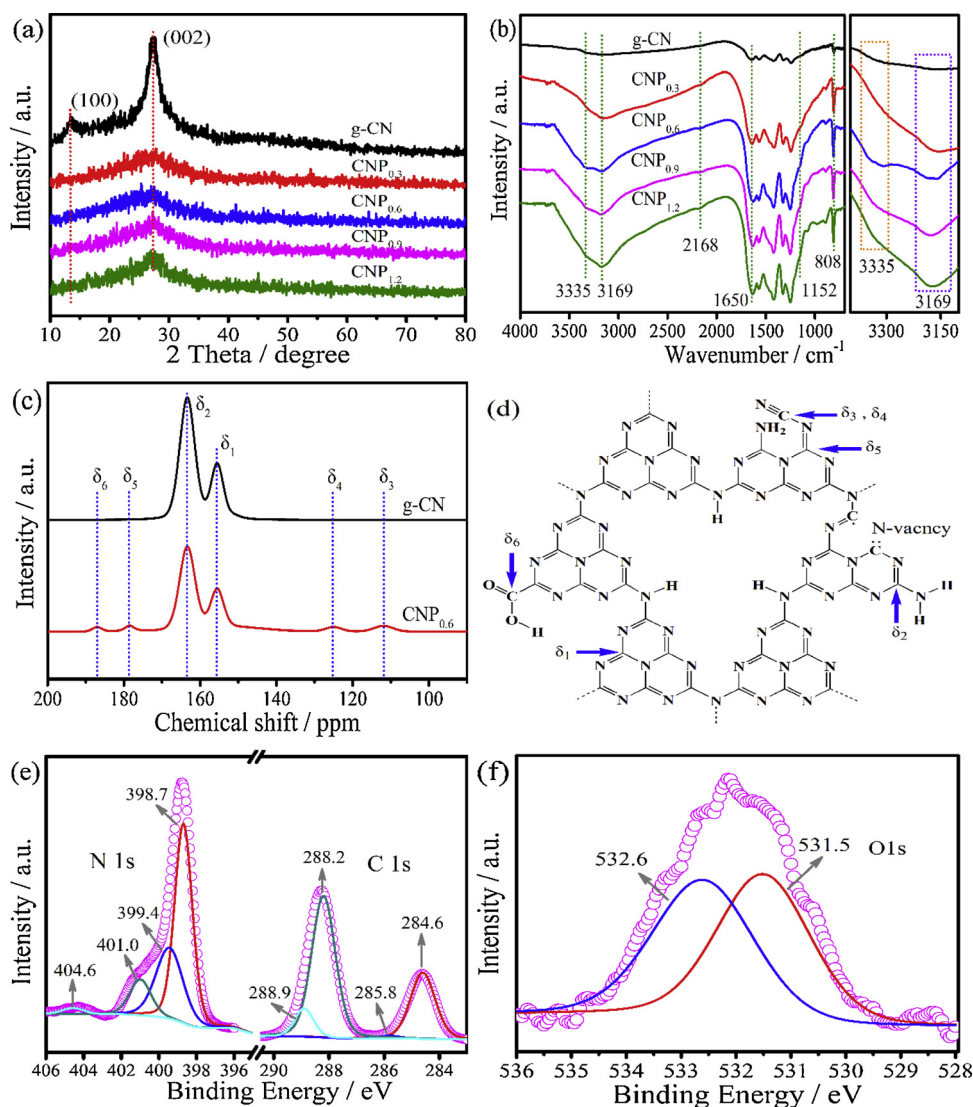


**Fig. 1.** (a) XRD patterns and (b) FTIR spectra for g-CN and CNPt ( $t = 0.3, 0.6, 0.9, 1.2$ ); (c) Solid-state <sup>13</sup>C magic angle spinning NMR spectra of g-CN and CNP<sub>0.6</sub>; (d) Proposed structure of tri-s-triazine units of CNPt; (e–f) High resolution C 1s, N 1s, O 1s XPS spectra of CNP<sub>0.6</sub>.

XPS spectra of CNN<sub>t</sub> and CNS<sub>t</sub> (Fig. S10-S11). These analysis results evidently confirmed the formation of N defects accompanied by the introduction to oxygen-containing defects in the tri-s-triazine framework of the as-fabricated carbon nitrides.

The morphological structures of as-fabricated carbon nitrides were investigated by SEM and TEM (Fig. 2). In Fig. 2a-b, the CNP<sub>t</sub> exhibit the hexagonal tubular structure with nanometer layered textures and amounts of flocculent body like cotton inside the tube. Meanwhile, the g-CN only shows an irregular bulk morphology (Fig. S12). The layered structures in CNP<sub>t</sub> tube derived from the original stacking of planar sheets via weak  $\pi$ - $\pi$  interactions in the hexagonal rod-like precursor. In the process of calcination, the  $\pi$ - $\pi$  interaction will be destroyed, the supramolecular precursor will shrink and stretch along the c-axis, resulting in the formation of layered structure accompanied by the formation of abundant mesoporous textures and flocculent body inside the tubular carbon nitride (Fig. 2c). The TEM element mapping (Fig. 2d) and EDX spectrum (Fig. S13) display the content of element P is still low, according with the XPS analysis content of 0.57 Atomic %. More important, the P 2p spectrum for CNP<sub>0.6</sub> is only fitted to a sole signal peak at 133.6 eV (Fig. S7b), corresponding to the characteristic signal of pentavalent tetracoordinated phosphorus [PO<sub>4</sub>] in phosphate compounds [60]. The results confirm that phosphoric acid mainly acts as a revulsant to promote the dissolution of melamine and in-situ hydrolysis

of melamine to form cyanuric acid, generating the hexagonal rod-like precursor, and further transformed into the hexagonal tubular carbon nitride under calcination condition. Other protonic acid assisted carbon nitrides CNN<sub>t</sub> and CNS<sub>t</sub> also exhibit the similar hexagonal tubular structures (Fig. S14-15). The more detailed formation process is discussed in the supporting information (Fig. S16-S17). N<sub>2</sub> adsorption-desorption measurement was carried out to further examine the pore textures and specific surface area. As expected, CNP<sub>t</sub> exhibits abundant mesoporous structure with pore sizes ranging from 2 to 9 nm, and an improved specific surface area of 59.68 m<sup>2</sup> g<sup>-1</sup>, much higher than that of g-CN (4.87 m<sup>2</sup> g<sup>-1</sup>) (Fig. 2e).

The unique hexagonal tubular structure of as-fabricated carbon nitrides promotes the formation of abundant N defects and oxygen-containing defects, and contribute to the exposure of more active sites. What's more, the tubular carbon nitride with abundant defects is expected to an ideal design for highly-efficient photocatalytic application because of the special advantages, such as, I) the unique one-dimensional tubular structure with layered structure and flocculent body inside can promote electron transfer rapidly; II) the hierarchical porous morphology can provide low-resistant diffusion channels to ensure fast mass exchanges between reactant molecules and product molecules; III) the abundant defects and increased specific area provide a high probability for the exposure of more active sites. All these favorable features

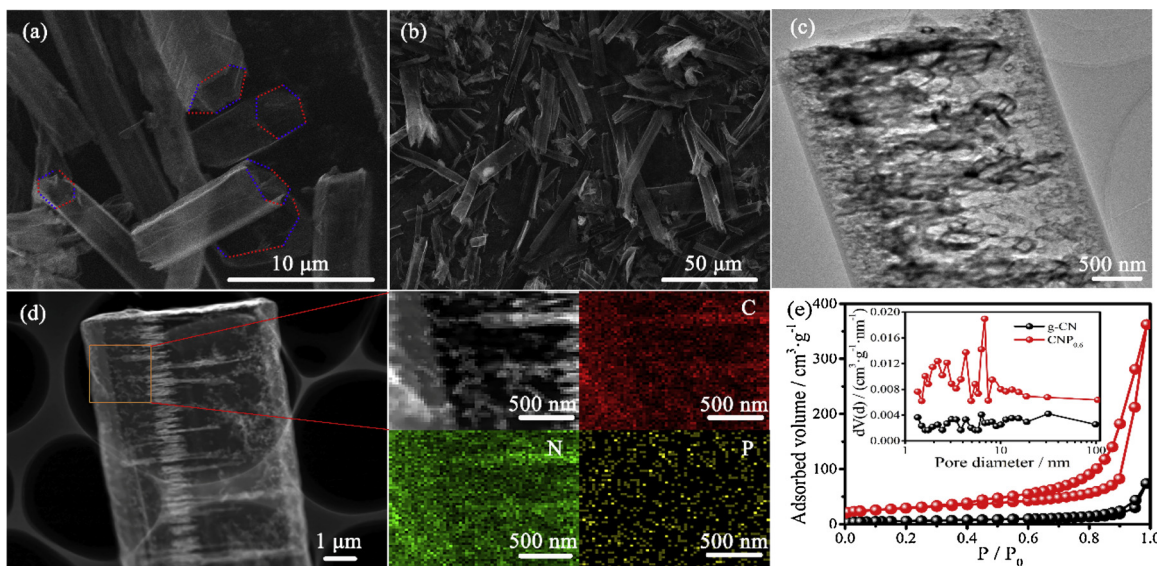


**Fig. 2.** (a–b) SEM images of hexagonal tubular carbon nitride CNP<sub>0.6</sub>; (c–d) TEM images of hexagonal tubular carbon nitride CNP<sub>0.6</sub> along with element mapping of C, N and P; (e) N<sub>2</sub> adsorption-desorption isotherm and corresponding pore-size distribution (insert) of g-CN and CNP<sub>0.6</sub>.

indicate that the hexagonal tubular carbon nitride with abundant defects can achieve highly-efficient photocatalytic applications.

## 2.2. Photoreduction and photooxidation performance

### 2.2.1. Photocatalytic H<sub>2</sub> evolution and CO<sub>2</sub> reduction

Photocatalytic H<sub>2</sub> evolution was first evaluated with triethanolamine (TEOA) and 3 wt % Pt as sacrificial agent and cocatalyst, respectively. As expected in Fig. 3a, the CNP<sub>t</sub> exhibit remarkable improved H<sub>2</sub> evolution ability, the largest H<sub>2</sub> evolution amount can reach 39.74 mmol·g<sup>-1</sup> in 5 h, which is 69.7 times higher than that of g-CN

(0.57 mmol·g<sup>-1</sup>). The corresponding turnover number (TON) is calculated to be 259.2. Note that CNP<sub>0.6</sub> catalyst shows high H<sub>2</sub> evolution activity in a range of 400–450 nm base on the variation tendencies of H<sub>2</sub> evolution rate (Fig. S18), and apparent quantum efficiency (AQE) is estimated to be 259.2 and 8.32% at 420 nm. The highly-efficient photocatalytic H<sub>2</sub> evolution activity was also achieved over CNN<sub>t</sub> and CNS<sub>t</sub> (Fig. S19–S20). As summarized in Table S4, all the tubular carbon nitride CNX<sub>t</sub> exhibit the significant enhanced photocatalytic H<sub>2</sub> rates in comparison with g-CN, and far higher than that of most reported carbon nitride photocatalysts (Table S5). The results confirm that the hexagonal tubular carbon nitride with abundant defects possess highly-

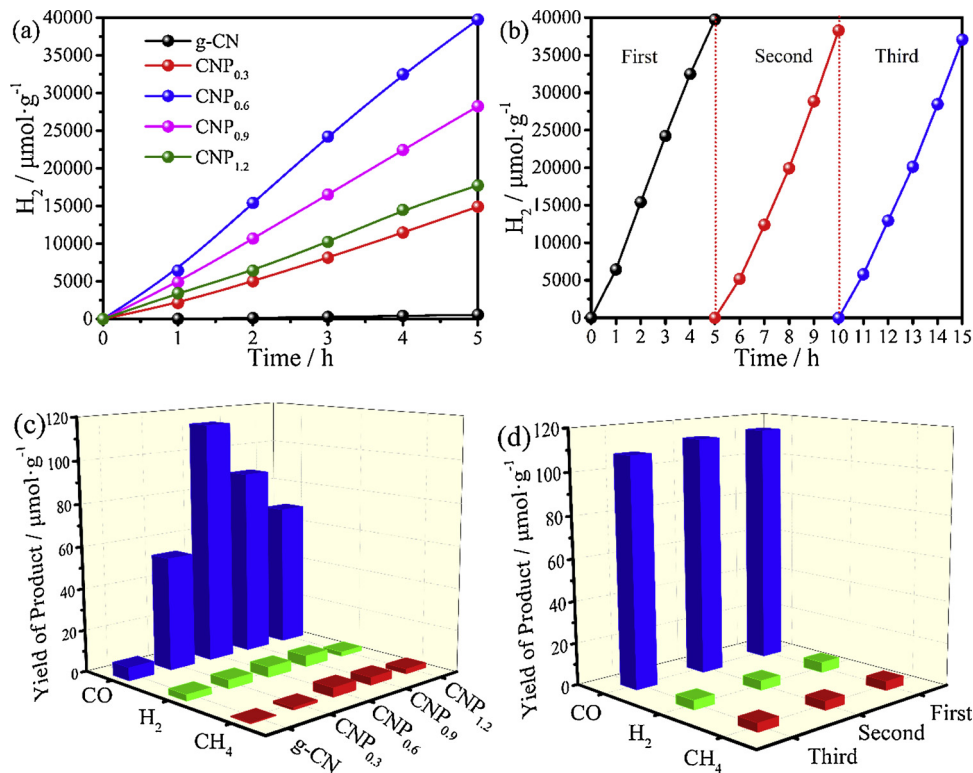


**Fig. 3.** (a) Photocatalytic H<sub>2</sub> evolution of g-CN and CNP<sub>t</sub> ( $t = 0.3, 0.6, 0.9, 1.2$ ); (b) Cyclic stability tests of optimal CNP<sub>0.6</sub>; (c) Photocatalytic CO<sub>2</sub> reduction performance over g-CN and CNP<sub>t</sub> ( $t = 0.3, 0.6, 0.9, 1.2$ ); (d) Photocatalytic CO<sub>2</sub> reduction for three consecutive runs.

efficient photocatalytic H<sub>2</sub> evolution performance, benefitting from unique structure control and defective surface design. In addition, the photocatalytic H<sub>2</sub> evolution tests for optimal CNP<sub>0.6</sub> were performed to evaluate its stability with intermittent degassing of the reaction every 5 h. In Fig. 3b, no obvious activity decrease could be observed after consecutive photocatalytic reaction of 15 h, suggesting the robust characteristic of the tubular carbon nitride CNX<sub>t</sub> towards the aqueous solution and visible light contact. After photocatalytic reaction, the photocatalyst was also characterized by XRD and FTIR (Fig. S21), no noticeable alternation was occurred for the structure of catalyst, again indicating the high stability of CNX<sub>t</sub> in the photocatalytic H<sub>2</sub> evolution reaction.

Subsequently, photocatalytic CO<sub>2</sub> reduction was carried out to prove the superiority of the tubular carbon nitride with abundant useful defects in water/methyl cyanide (MeCN)/ triethanolamine (TEOA) mixture. MeCN was used as the major solvent due to its high CO<sub>2</sub> solubility under mild reaction conditions. For all the photocatalyst investigated, the H<sub>2</sub>, CO and CH<sub>4</sub> was detected, but the photocatalytic system exhibits an excellent selectivity for CO generation. As shown in Fig. 3c, the CO generation over CNP<sub>t</sub> presents gaussian distribution. The highest CO generation amount can reach 114.28 μmol g<sup>-1</sup> after 12 h of photocatalytic reaction, much higher than that of g-CN (6.35 μmol g<sup>-1</sup>). It can be observed that CNP<sub>0.6</sub> catalyst gives high CO generation rate ranging from 400 to 450 nm base on the variation tendencies of CO formation rate (Fig. S22). In theory, the conduct band potential of carbon nitride is thermodynamically more sufficient for CO<sub>2</sub> reduction to CH<sub>4</sub> than CO, but the formation of CH<sub>4</sub> needs a series of elementary reaction steps through CO as the intermediate, involving eight electron transfer in the elementary steps. Thus, the subsequent elementary reaction after CO formation cannot perform sufficiently rapidly before CO desorbs from the surface of the tubular carbon nitride, resulting in CO as the main product. The detailed discussion is in supporting information. Such results have also been observed in other reported semiconductor photocatalyst [61]. Other products (e.g., CH<sub>3</sub>OH, HCOOH and CH<sub>3</sub>CH<sub>2</sub>OH) were not detected. Moreover, contrast experiment using Ar gas under the same experiment condition was also performed, no product was observed. The CNN<sub>t</sub> and CNN<sub>t</sub> also exhibit the enhanced CO formation capacity (Fig. S23-S24). Among them, the CNP<sub>0.6</sub> shows the best photocatalytic CO<sub>2</sub> reduction ability with 92.4% CO selectivity. The average CO formation rate for CNP<sub>0.6</sub> can reach 9.52 μmol g<sup>-1</sup> h<sup>-1</sup>, better than that of most reported carbon nitride base photocatalysts (Table S6). Therefore, these results confirmed that CO formation is ascribed to the photocatalytic CO<sub>2</sub> reduction. Their excellent photocatalytic stability was confirmed by three cycle tests (Fig. 3d). Moreover, the XRD patterns and FTIR spectra of CNP<sub>0.6</sub> before and after photocatalytic test (Fig. S25) show no obvious changes in the crystal structure and chemical functional groups, further indicating the hexagonal tubular carbon nitride with abundant defects is rather stable against the reaction condition of CO<sub>2</sub> reduction.

### 2.2.2. Photocatalytic NO oxidation

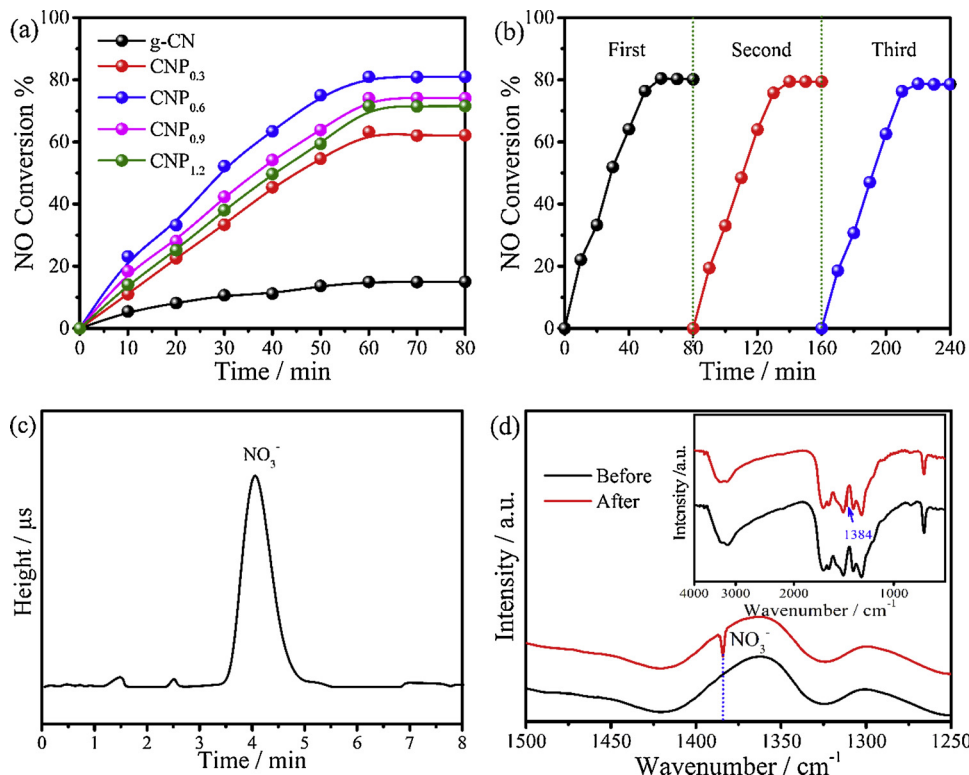
In addition to the highly-efficient photocatalytic reduction capacity shown by the hexagonal tubular carbon nitride with abundant defects as confirmed above, a striking change in photocatalytic oxidation capacity, associated with photoexcited electrons and holes, was also observed, by comparing the photocatalytic oxidation behaviors of NO with g-CN and CNX<sub>t</sub> (Fig. 4a and Fig. S26-S27). It is worth emphasizing that NO oxidation could be negligent in the absence of visible light, photocatalyst, H<sub>2</sub>O<sub>2</sub> solution, both photocatalyst and H<sub>2</sub>O<sub>2</sub> solution, respectively (Fig. S28). The control experimental results accord with our previous work [62,63]. The NO (~ 400 ppm) can be efficiently removed by CNX<sub>t</sub> with 80 min in the presence of visible light, while only lower NO removal efficiency occurs by g-CN. Note that the NO oxidation efficiency first increases with light irradiation time and then reaches chemical equilibrium. All the tubular carbon nitrides CNX<sub>t</sub> showed the excellent photocatalytic NO removal efficiency in

comparison with g-CN (Table S7). Among them, the CNP<sub>0.6</sub> exhibit the largest NO removal rate of 81.97%, increasing by 65.95% than that of g-CN. Their excellent photocatalytic NO oxidation stability was proved by three cycle tests in despite of the slight activity loss (Fig. 4b). Furthermore, the tubular carbon nitrides with abundant defects possess the excellent oxidation capacity for high concentration NO at ppm level than most reported photocatalysts (Table S8), which exhibit the huge potential advantage for the removal of NO from coal flue gas in the future. It is worth noting that the residence time, light intensity, reaction time, etc. have strongly influence on the efficiency of photocatalytic NO removal through the comparison. After photocatalytic NO oxidation, the NO<sub>3</sub><sup>-</sup> was detected to be the reaction product as confirmed by ion chromatography and FTIR (Fig. 4c-d). The nitrogen balance calculation was further performed to explore the possible by-products (Section 1, supporting information). The result further illustrated that NO<sub>3</sub><sup>-</sup> is the reaction product in photocatalytic NO oxidation. Furthermore, the fluorescence spectra and the trapping experiments confirm superoxide radicals (O<sub>2</sub><sup>-</sup>) play the leading role in the process of NO oxidation. The more detailed analysis is in the supporting information (Fig. S29-S30).

### 2.3. Optical properties and electronic structure analysis

To further identify the highly-efficient photocatalytic performance of the tubular carbon nitride with abundant defects, their optical properties were studied by UV-vis absorption spectroscopy (Fig. 5a and Fig. S31-S32). It can be observed that the sharp absorption band thresholds of CNX<sub>t</sub> exhibit a blue shift in comparison with g-CN, showing an increased band gap energy of 2.85 ± 0.05 eV (Table S9), which originates from the strong effect of quantum confinement [64]. Furthermore, a broader light absorption tail in the visible light region and even the infrared region, is also observed. The increased optical absorption capacity of CNP<sub>t</sub> results from the existence of defective states [65,66]. The Mott-Schottky (MS) plots (Fig. 5b) reveal the conduction band potentials of g-CN and CNP<sub>0.6</sub> are respectively -1.09 and -1.13 V versus normal hydrogen electrode (NHE), corresponding valence band potentials are 1.67 and 1.77 V, respectively, similar to previous report [60,67]. Therefore, the tubular carbon nitrides with abundant defects possess the increased band gap energies and enhanced light harvesting ability, thus contributing to highly-efficient photocatalytic H<sub>2</sub> evolution, CO<sub>2</sub> reduction, and NO oxidation, simultaneously.

The highly-efficient photocatalytic performance of the tubular carbon nitride with abundant defects also benefits from their fast photoexcited charge transfer and migration ability as confirmed by photoluminescence (PL) spectra, time-resolved photoluminescence, transient photocurrents and electrochemical impedance spectroscopy. As observed in Fig. 5c, g-CN exhibits a strong and wide PL emission peak at ca. 460 nm, while the CNP<sub>t</sub> exhibits a tremendous reduced peak intensity with a redshift, indicating highly-efficient separation and transfer of photoexcited carriers. The improved charge separation should be attributed to the unique structure of the tubular carbon nitride, that's because the unique tubular structure can significantly reduce the diffusion length of charge migration, and promote electron relocalization on surface terminal sites, especially at the 2D planar edges/tips to suppress the recombination of photoinduced charges [68]. According to the time-resolved photoluminescence analysis result (Fig. 5d), the CNP<sub>t</sub> possess longer average fluorescence lifetime ( $\tau_a$ ) than that of g-CN (10.13 vs. 3.88 ns), according with to previous reports [69,70]. The enhanced charge migration is intuitively verified by higher photocurrent density during on-off cycles of intermittent visible light and the smaller charge migration resistance (Fig. S30). Simultaneously, the improved photocurrent density and decreased charge migration resistance were also observed over CNN<sub>t</sub> and CNS<sub>t</sub> (Fig. S33-S35), demonstrating that all of them possess enhanced charge separation and transfer ability, thus achieving highly-efficient photocatalytic



performance for H<sub>2</sub> evolution, CO<sub>2</sub> reduction and NO removal for all the unique hexagonal tubular carbon nitrides.

#### 2.4. Photocatalytic reduction and oxidation mechanism

The photocatalytic performance discrepancy for CNP<sub>t</sub>, CNN<sub>t</sub> and CNS<sub>t</sub> should be attributed to the optimization level of the aromatic π-conjugated system in the defect abundant hexagonal tubular carbon nitride, resulting in a more significantly reduced recombination

probability of charge carriers and more fast charge separation efficiency as discussed above, which finally affect the photocatalytic performance.

Both photocatalytic H<sub>2</sub> evolution and CO<sub>2</sub> reduction are the direct reactions involving photoexcited electrons and holes (Fig. 5e, left). H<sub>2</sub> evolution is the process of proton reduction. Under visible light irradiation, photogenerated electrons will transfer to the catalyst surface, and react with protons to generate H<sub>2</sub>, while the holes oxidize the TEOA to form TEOA<sup>+</sup>, thus promoting H<sub>2</sub> generation smoothly. CO<sub>2</sub> reduction is the proton-assisted transfer process of multiple electrons. The E<sub>CB</sub>

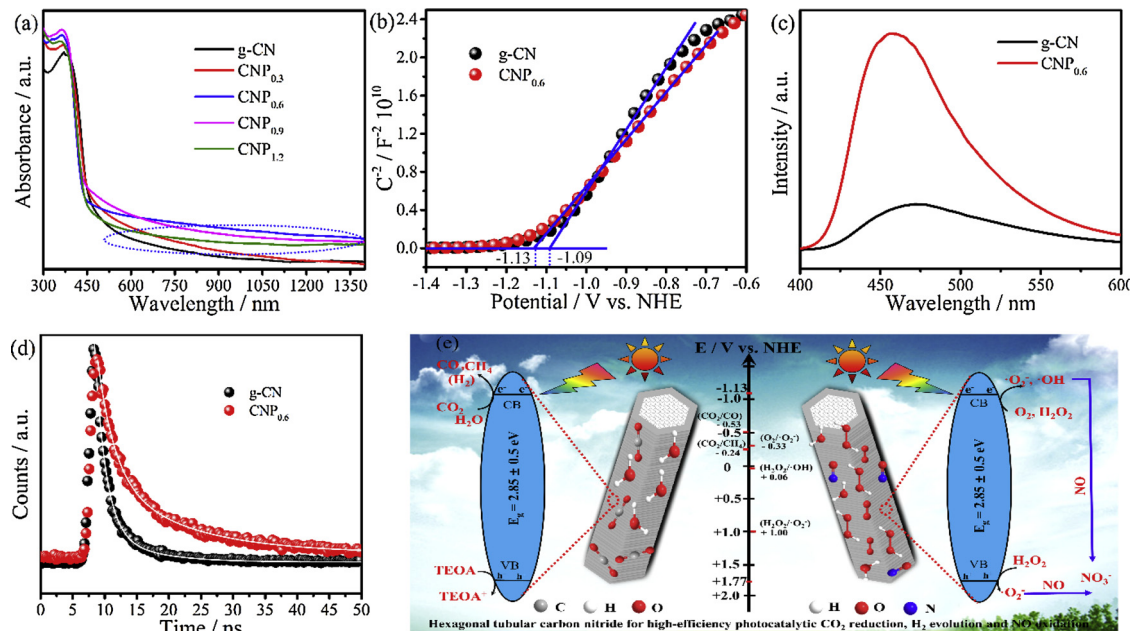


Fig. 5. (a) UV-vis diffuse reflection spectra of g-CN and CNP<sub>t</sub>; (b) Mott-Schottky (MS) plots of g-CN and CNP<sub>0.6</sub>; (c) Photoluminescence (PL) spectra of g-CN and CNP<sub>0.6</sub>; (d) Time-resolved PL decay spectra of g-CN and CNP<sub>0.6</sub>; (e) Schematic illustration of photocatalytic mechanism of photocatalytic H<sub>2</sub> evolution, CO<sub>2</sub> reduction, and NO oxidation.

potential of CN<sub>x</sub> is sufficient to reduce CO<sub>2</sub> to form various products as discussed above. However, the CO can be more easily generated in the system, which is because the formation of other products needs more than two electrons via a series of elementary steps. CO<sub>2</sub> reduction to CO is dynamically favored processes in fact. Note that CO<sub>2</sub> reduction is accompanied by slight H<sub>2</sub> evolution as a competing reaction. As photocatalytic reaction proceeds, the holes on the valence band are consumed by the oxidation of TEOA, thus restraining the charge recombination, the large amounts of photoexcited electrons accumulated on the conduction band will reduce CO<sub>2</sub> to CO and CH<sub>4</sub>, in which CO is the main product.

Photocatalytic NO oxidation is the indirect reaction involving photoexcited electrons and holes, which oxidize and reduce the additive species (e.g., O<sub>2</sub>, H<sub>2</sub>O, H<sub>2</sub>O<sub>2</sub>) to produce active free radicals (Fig. 5e, right). In the NO oxidation, the common active species include superoxide radicals (·O<sub>2</sub><sup>-</sup>), hydroxyl radicals (·OH) and holes (h<sup>+</sup>). Then these formed active free radicals react with NO on the catalyst surface to form other substances. However, the involving active species and reaction mechanism in different photocatalytic systems are discrepant. Herein, ·O<sub>2</sub><sup>-</sup> is the main active species and plays a dominant role, along with more production and participation of active species (especially for ·O<sub>2</sub><sup>-</sup>) because of introduction to H<sub>2</sub>O<sub>2</sub>, which accelerates ·O<sub>2</sub><sup>-</sup> reacting with NO to achieve high removal efficiency of NO (~ 400 ppm), and generate nitrate (NO<sub>3</sub><sup>-</sup>) simultaneously.

### 3. Conclusions

In summary, the hexagonal tubular carbon nitride with abundant nitrogen defects and oxygen-containing defects have been successfully prepared by using melamine and acid as starting material and reductive under hydrothermal condition. The resultant hexagonal tubular carbon nitride with abundant defects shows highly-efficient photocatalytic performance on H<sub>2</sub> evolution and CO<sub>2</sub> reduction. The H<sub>2</sub> evolution rate can reach 7.95 mmol·g<sup>-1</sup> h<sup>-1</sup> under visible light, 69.7 times higher than that of g-CN. The corresponding turnover number (TON) and apparent quantum efficiency (AQE) are calculated to be 259.2 and 8.32% at 420 nm, respectively. For CO<sub>2</sub> reduction, the photocatalytic system achieves 114.28 μmol g<sup>-1</sup> CO product with 92.4% selectivity. Moreover, the hexagonal tubular carbon nitride also exhibits excellent visible light photocatalytic NO removal efficiency of 81.97%, increasing by 65.95% than that of g-CN. The highly-efficient photocatalytic activities benefit from the unique structure of the hexagonal tubular carbon nitride with abundant defects, accompanying with the increased specific surface area, exposure of more active sites, enhanced light absorption capacity, improved redox ability, improved photogenic electron-hole separation. The systematic work has revealed the significance of defect abundant tubular structure in achieving highly-efficient multifunction photocatalytic applications of carbon nitride, supplying a universal and feasible acid-assisted synthetic route to synthesize highly-efficient tubular carbon nitride with abundant useful defects for alleviating environmental and energy issues in the future.

### 4. Experimental section

The detailed experimental section has been shown in Supporting Information.

### Declaration of Competing Interest

The authors declare that they have no known competing financial interests or personal relationships that could have appeared to influence the work reported in this paper.

### Acknowledgements

This work was financially supported by the Key Project of Chinese

National Programs for Research and Development (2016YFC0203800), the National Natural Science Foundation of China (51578288), Jiangsu Province Scientific and Technological Achievements into a Special Fund Project (BA2016055 and BA2017095), Top-notch Academic Programs Project of Jiangsu Higher Education Institutions, A Project by the Priority Academic Program Development of Jiangsu Higher Education Institutions, Postgraduate Research & Practice Innovation Program of Jiangsu Province (KYCX18\_0443) and the China Scholarship Council (CSC) program.

### Appendix A. Supplementary data

Supplementary material related to this article can be found, in the online version, at doi:<https://doi.org/10.1016/j.apcatb.2019.118011>.

### References

- [1] A. Kudo, Y. Miseki, Heterogeneous photocatalyst materials for water splitting, *Chem. Soc. Rev.* 38 (2009) 253–278.
- [2] D.R. Feldman, W.D. Collins, P.J. Gero, M.S. Torn, E.J. Mlawer, T.R. Shippert, Observational determination of surface radiative forcing by CO<sub>2</sub> from 2000 to 2010, *Nature* 519 (2015) 339–343.
- [3] E.V. Eynde, B. Lenaerts, T. Tytgat, R. Blust, S. Lenaerts, Valorization of flue gas by combining photocatalytic gas pretreatment with microalgae production, *Environ. Sci. Technol.* 50 (2016) 2538–2545.
- [4] J.K. Stolarczyk, S. Bhattacharyya, L. Polavarapu, J. Feldmann, Challenges and prospects in solar water splitting and CO<sub>2</sub> reduction with inorganic and hybrid nanostructures, *ACS Catal.* 8 (2018) 3602–3635.
- [5] S.P. Wan, M. Ou, Q. Zhong, S.L. Zhang, W. Cai, Supramolecular synthesis of multifunctional holey carbon nitride nanosheet with high-efficiency photocatalytic performance, *Adv. Optical Mater.* (2017) 2700536.
- [6] M. Ou, W.G. Tu, S.M. Yin, W.N. Xing, S.Y. Wu, H.J. Wang, S.P. Wan, Q. Zhong, R. Xu, Amino-assisted anchoring of CsPbBr<sub>3</sub> perovskite quantum dots on porous g-C<sub>3</sub>N<sub>4</sub> for enhanced photocatalytic CO<sub>2</sub> reduction, *Angew. Chem.* 130 (2018) 13758–13762.
- [7] L. Wang, K. Xu, W. Cui, D.D. Lv, L. Wang, L. Ren, X. Xu, F. Dong, S.X. Dou, W.C. Hao, Y. Du, Monolayer epitaxial heterostructures for selective visible-light-driven photocatalytic NO oxidation, *Adv. Funct. Mater.* (2019) 1808084.
- [8] W. Cai, Q. Zhong, W. Zhao, Y.F. Bu, Focus on the modified Ce<sub>x</sub>Zr<sub>1-x</sub>O<sub>2</sub> with the rigid benzene-muti-carboxylate ligands and its catalysis in oxidation of NO, *Appl. Catal. B: Environ.* 158–159 (2014) 258–268.
- [9] Y. Wang, L. Tan, M.H. Tan, P.P. Zhang, Y. Fang, Y. Yoneyama, G.H. Yang, N. Tsubaki, Rationally designing bifunctional catalysts as an efficient strategy to boost CO<sub>2</sub> hydrogenation producing value-added aromatics, *ACS Catal.* 9 (2019) 895–901.
- [10] D.D. Zhu, J.L. Liu, S.Z. Qiao, Recent advances in inorganic heterogeneous electrocatalysts for reduction of carbon dioxide, *Adv. Mater.* 28 (2016) 3423–3452.
- [11] H.P. Wang, X.B. Li, L. Gao, H.L. Wu, J. Yang, L. Cai, T.B. Ma, C.H. Tung, L.Z. Wu, G. Yu, Three-dimensional graphene networks with abundant sharp edge sites for efficient electrocatalytic hydrogen evolution, *Angew. Chem.* 130 (2018) 198–203.
- [12] Y. Li, K. Yin, L.L. Wang, X.L. Lu, Y.Q. Zhang, Y.T. Liu, D.F. Yan, Y.Z. Song, S.L. Luo, Engineering MoS<sub>2</sub> nanomesh with holes and lattice defects for highly active hydrogen evolution reaction, *Appl. Catal. B: Environ.* 239 (2018) 537–544.
- [13] A. Fujishima, K. Honda, Electrochemical photolysis of water at a semiconductor electrode, *Nature* 238 (1972) 37–38.
- [14] X.C. Wang, K. Maeda, A. Thomas, K. Takanabe, G. Xin, J. Carlsson, J.K. Domen, M.A. Antonietti, Metal-free polymeric photocatalyst for hydrogen production from water under visible light, *Nat. Mater.* 8 (2009) 76–80.
- [15] T. Takata, K. Domen, Particulate photocatalysts for water splitting: recent advances and future prospects, *ACS Energy Lett.* 4 (2019) 542–549.
- [16] L. Yao, A. Rahamanudin, N. Guijarro, K. Sivula, Organic semiconductor based devices for solar water splitting, *Adv. Energy Mater.* 8 (2018) 1802585.
- [17] M.F. Kuehnel, K.L. Orchard, K.E. Dalle, E. Reisner, Selective photocatalytic CO<sub>2</sub> reduction in water through anchoring of a molecular Ni catalyst on CdS nanocrystals, *J. Am. Chem. Soc.* 139 (2017) 7217–7223.
- [18] S.P. Wan, M. Ou, Q. Zhong, X.M. Wang, Perovskite-type CsPbBr<sub>3</sub> quantum dots/Uio-66(NH<sub>2</sub>) nanojunction as efficient visible-light-driven photocatalyst for CO<sub>2</sub> reduction, *Chem. Eng. J.* 358 (2019) 1287–1295.
- [19] C.C. Wang, J.R. Li, X.L. Lv, Y.Q. Zhang, G.S. Guo, Photocatalytic organic pollutants degradation in metal-organic frameworks, *Energy Environ. Sci.* 7 (2014) 2831–2867.
- [20] Y. Markushyna, C. Teutloff, B. Kurpil, D. Cruz, I. Lauermann, Y.B. Zhao, M. Antonietti, A. Savateev, Halogenation of aromatic hydrocarbons by halide anion oxidation with poly (heptazine imide) photocatalyst, *Appl. Catal. B: Environ.* 248 (2019) 211–217.
- [21] B. Kurpil, K. Otte, A. Mishchenko, P. Lamagni, W. Lipiński, N. Lock, M. Antonietti, A. Savateev, Carbon nitride photocatalyzes regioselective aminium radical addition to the carbonyl bond and yields N-fused pyrroles, *Nat. Commun.* 10 (2019) 945.
- [22] B. Kurpil, Y. Markushyna, A. Savateev, Visible-light-driven reductive (cyclo)dimmerization of chalcones over heterogeneous carbon nitride photocatalyst, *ACS*

- Catal. 9 (2019) 1531–1538.
- [23] S.W. Cao, J.X. Low, J.G. Yu, M. Jaroniec, Polymeric photocatalysts based on graphitic carbon nitride, *Adv. Mater.* 27 (2015) 2150–2176.
- [24] C. Cometto, R. Kuriki, L.J. Chen, K. Maeda, T.C. Lau, O. Ishitani, M. Robert, A carbon nitride/Fe quaterpyridine catalytic system for photostimulated CO<sub>2</sub>-to-CO conversion with visible light, *J. Am. Chem. Soc.* 140 (2018) 7437–7440.
- [25] Y.Z. Zhao, S.C. Zong, C. Cheng, J.W. Shi, P.H. Guo, X.J. Guan, B. Luo, S.H. Shen, L.J. Guo, Rapid high-temperature treatment on graphitic carbon nitride for excellent photocatalytic H<sub>2</sub>-evolution performance, *Appl. Catal. B: Environ.* 233 (2018) 80–87.
- [26] Z. Yang, Y.J. Zhang, Z. Schnepf, Soft and hard templating of graphitic carbon nitride, *J. Mater. Chem. A* 3 (2015) 14081–14092.
- [27] L.B. Jiang, X.Z. Yuan, Y. Pan, J. Liang, G.M. Zeng, Z.B. Wu, H. Wang, Doping of graphitic carbon nitride for photocatalysis: a review, *Appl. Catal. B: Environ.* 217 (2017) 388–406.
- [28] W. Che, W.R. Cheng, T. Yao, F.M. Tang, W. Liu, H. Su, Y.Y. Huang, Q.H. Liu, J.K. Liu, F.C. Hu, Z.Y. Pan, Z.H. Sun, S.Q. Wei, Fast photoelectron transfer in (C<sub>ring</sub>)<sub>n</sub>C<sub>3</sub>N<sub>4</sub> plane heterostructural nanosheets for overall water splitting, *J. Am. Chem. Soc.* 139 (2017) 3021–3026.
- [29] F.K. Kessler, Y. Zheng, D. Schwarz, C. Merschjann, W. Schnick, X.C. Wang, M.J. Bojdys, Functional carbon nitride materials—design strategies for electrochemical devices, *Nat. Rev. Mater.* 2 (2017) 17030.
- [30] C. Cheng, J.W. Shi, Y.C. Hu, L.J. Guo, WO<sub>3</sub>/g-C<sub>3</sub>N<sub>4</sub> composites: one-pot preparation and enhanced photocatalytic H<sub>2</sub> production under visible-light irradiation, *Nanotechnology* 28 (2017) 164002.
- [31] H.L. Jiang, X.Q. Li, M.L. Li, P.P. Niu, T. Wang, D.Z. Chen, P.H. Chen, J.P. Zou, A new strategy for triggering photocatalytic activity of cytochrome P450 by coupling of semiconductors, *Chem. Eng. J.* 358 (2019) 58–66.
- [32] M.K. Bhunia, S. Melissen, M.R. Parida, P. Sarawade, J.M. Basset, D.H. Anjum, O.F. Mohammed, P. Sautel, T.L. Bahers, K. Takanabe, Dendritic tip-on polytriazine-based carbon nitride photocatalyst with high hydrogen evolution activity, *Chem. Mater.* 27 (2015) 8237–8247.
- [33] N.Q. Wu, J. Wang, D.N. Tafen, H. Wang, J.G. Zheng, J.P. Lewis, X.G. Liu, S.S. Leonard, A. Manivannan, Shape-enhanced photocatalytic activity of single-crystalline anatase TiO<sub>2</sub> (101) nanobelts, *J. Am. Chem. Soc.* 132 (2010) 6679–6685.
- [34] G.K. Mor, K. Shankar, M. Paulose, O.K. Varghese, C.A. Grimes, Use of highly-ordered TiO<sub>2</sub> nanotube arrays in dye-sensitized solar cells, *Nano Lett.* 6 (2006) 215–218.
- [35] V.W. Lau, I. Moudrakovski, T. Botari, S. Weinberger, M.B. Mesch, V. Duppel, J. Senker, V. Blum, B.V. Lotsch, Rational design of carbon nitride photocatalysts by identification of cyanamide defects as catalytically relevant sites, *Nat. Commun.* 7 (2016) 12165.
- [36] M.B. Chambers, X. Wang, L. Ellezam, O. Ersen, M. Fontecave, C. Sanchez, L. Rozes, C. Molot-Dražnić, Maximizing the photocatalytic activity of metal-organic frameworks with aminated-functionalized linkers: stoichiometric effects in MIL-125-NH<sub>2</sub>, *J. Am. Chem. Soc.* 139 (2017) 8222–8228.
- [37] L. Shi, L.Q. Yang, W. Zhou, Y.Y. Liu, L.S. Yin, X. Hai, H. Song, J.H. Ye, Photoassisted construction of holey defective g-C<sub>3</sub>N<sub>4</sub> photocatalysts for efficient visible-light-driven H<sub>2</sub>O<sub>2</sub> production, *Small* 14 (2018) 1703142.
- [38] H.H. Ou, P.J. Yang, L.H. Lin, M. Anpo, X.C. Wang, Carbon nitride aerogels for the photoredox conversion of water, *Angew. Chem. Int. Ed.* 56 (2017) 10905–10910.
- [39] S.P. Wan, Q. Zhong, M. Ou, S.L. Zhang, Highly efficient simulated solar-light photocatalytic oxidation of gaseous NO with porous carbon nitride from copolymerization with thymine and mechanistic analysis, *RSC Adv.* 6 (2016) 101208–101215.
- [40] S.E. Guo, Z.P. Deng, M.X. Li, B.J. Jiang, C.G. Tian, Q.J. Pan, H.G. Fu, Phosphorus-doped carbon nitride tubes with a layered micronanostructure for enhanced visible-light photocatalytic hydrogen evolution, *Angew. Chem. Int. Ed.* 55 (2016) 1830–1834.
- [41] Y.C. Lu, J. Chen, A.J. Wang, N. Bao, J.J. Feng, W.P. Wang, L.X. Shao, Facile synthesis of oxygen and sulfur co-doped graphitic carbon nitride fluorescent quantum dots and their application for mercury(II) detection and bioimaging, *J. Mater. Chem. C* 3 (2015) 73–78.
- [42] P.F. Xia, M. Antonietti, B.C. Zhu, T. Heil, J.G. Yu, S.W. Cao, Designing defective crystalline carbon nitride to enable selective CO<sub>2</sub> photoreduction in the gas phase, *Adv. Funct. Mater.* (2019) 1900093.
- [43] D. Sun, R. Ban, P.H. Zhang, G.H. Wu, J.R. Zhang, J.J. Zhu, Hair fiber as a precursor for synthesizing of sulfur- and nitrogen-co-doped carbon dots with tunable luminescence properties, *Carbon* 64 (2013) 424–434.
- [44] D. Qu, M. Zheng, P. Du, Y. Zhou, L.G. Zhang, D. Li, H.Q. Tan, Z. Zhao, Z.G. Xie, Z.C. Sun, Highly luminescent S, N co-doped graphene quantum dots with broad visible absorption bands for visible light photocatalysts, *Nanoscale* 5 (2013) 12272–12277.
- [45] Y.X. Wang, H. Wang, F.Y. Chen, F. Cao, X.H. Zhao, S.G. Meng, Y.J. Cui, Facile synthesis of oxygen doped carbon nitride hollow microsphere for photocatalysis, *Appl. Catal. B: Environ.* 206 (2017) 417–425.
- [46] P. Zhang, D.R. Sun, A. Cho, S. Weon, S. Lee, J. Lee, J.W. Han, D.P. Kim, W.Y. Choi, Modified carbon nitride nanzyme as bifunctional glucose oxidase-peroxidase for metal-free bioinspired cascade photocatalysis, *Nat. Commun.* 10 (2019) 940.
- [47] N.N. Meng, J. Ren, Y. Liu, Y. Huang, T. Petit, B. Zhang, Engineering oxygen-containing and amino groups into two-dimensional atomically-thin porous polymeric carbon nitrogen for enhanced photocatalytic hydrogen production, *Energy Environ. Sci.* 11 (2018) 566–571.
- [48] B. Jürgens, E. Irran, J. Senker, P. Kroll, H. Müller, W. Schnick, Melem (2,5,8-triamino-tri-s-triazine), an important intermediate during condensation of melamine rings to graphitic carbon nitride: synthesis, structure determination by X-ray powder diffractometry, solid-state NMR, and theoretical studies, *J. Am. Chem. Soc.* 125 (2003) 10288–10300.
- [49] C.T. Qu, Y.S. Xu, X. Fan, D. Xu, R. Tandiana, X. Ling, Y.N. Jiang, C.B. Liu, L. Yu, W. Chen, C.L. Su, Highly crystalline K-intercalated polymeric carbon nitride for visible-light photocatalytic alkenes and alkynes deuterations, *Adv. Sci.* 6 (2019) 1801403.
- [50] H.J. Yu, R. Shi, Y.X. Zhao, T. Bian, Y.F. Zhao, C. Zhou, G.I.N. Waterhouse, L.Z. Wu, C.H. Tung, T.R. Zhang, Alkali-assisted synthesis of nitrogen deficient graphitic carbon nitride with tunable band structures for efficient visible-light-driven hydrogen evolution, *Adv. Mater.* 29 (2017) 1605148.
- [51] H.L. Gao, S.C. Yan, J.J. Wang, Y.A. Huang, P. Wang, Z.S. Li, Z.G. Zou, Towards efficient solar hydrogen production by intercalated carbon nitride photocatalyst, *Phys. Chem. Chem. Phys.* 15 (2013) 18077–18084.
- [52] Z.P. Song, T.R. Lin, L.H. Lin, S. Lin, F.F. Fu, X.C. Wang, L.Q. Guo, Invisible security ink based on water-soluble graphitic carbon nitride quantum dots, *Angew. Chem. Int. Ed.* 55 (2016) 2773–2777.
- [53] L.F. Ming, H. Yue, L.M. Xu, F. Chen, Hydrothermal synthesis of oxidized g-C<sub>3</sub>N<sub>4</sub> and its regulation of photocatalytic activity, *J. Mater. Chem. A* 2 (2014) 19145–19149.
- [54] P. Chen, T.Y. Xiao, Y.H. Qian, S.S. Li, S.H. Yu, A nitrogen-doped graphene/carbon nanotube nanocomposite with synergistically enhanced electrochemical activity, *Adv. Mater.* 25 (2013) 3192–3196.
- [55] P. Lampraserikun, A. Krittayavathananon, M. Sawangphruk, N-doped reduced graphene oxide aerogel coated on carboxyl modified carbon fiber paper for high-performance ionic-liquid supercapacitors, *Carbon* 102 (2016) 455–461.
- [56] Y.Y. Zhou, L. Zhang, W.Z. Wang, Direct functionalization of methane into ethanol over copper modified polymeric carbon nitride via photocatalysis, *Nat. Commun.* 10 (2019) 506.
- [57] Z.H. Hong, B. Shen, Y.L. Chen, B.Z. Lin, B.F. Gao, Enhancement of photocatalytic H<sub>2</sub> evolution over nitrogen-deficient graphitic carbon nitride, *J. Mater. Chem. A* 1 (2013) 11754–11761.
- [58] C.D. Lv, Y.M. Qian, C.S. Yan, Y. Ding, Y.Y. Liu, G. Chen, G.H. Yu, Defect engineering metal-free polymeric carbon nitride electrocatalyst for effective nitrogen fixation under ambient conditions, *Angew. Chem. Int. Ed.* 57 (2018) 10246–10250.
- [59] G.H. Dong, W.K. Ho, C.Y. Wang, Selective photocatalytic N<sub>2</sub> fixation dependent on g-C<sub>3</sub>N<sub>4</sub> induced by nitrogen vacancies, *J. Mater. Chem. A* 3 (2015) 23435–23441.
- [60] L. Shi, K. Chang, H.B. Zhang, X. Hai, L.Q. Yang, T. Wang, J.H. Ye, Drastic enhancement of photocatalytic activities over phosphoric acid protonated porous g-C<sub>3</sub>N<sub>4</sub> nanosheets under visible light, *Small* 12 (2016) 4431–4439.
- [61] O.K. Varghese, M. Paulose, T.J. LaTempa, C.A. Grimes, High-rate solar photocatalytic conversion of CO<sub>2</sub> and water vapor to hydrocarbon fuels, *Nano Lett.* 9 (2009) 731–737.
- [62] S.P. Wan, Q. Zhong, M. Ou, S.L. Zhang, W. Cai, Facial synthesis of sheet-like carbon nitride from preorganized hydrogen bonded supramolecular precursors and its high efficient photocatalytic oxidation of gas-phase NO, *J. Photochem. Photobiol. A: Chem.* 340 (2017) 136–145.
- [63] M. Ou, S.P. Wan, Q. Zhong, S.L. Zhang, Y. Song, L.N. Guo, W. Cai, Y.L. Xu, Hierarchical Z-scheme photocatalyst of g-C<sub>3</sub>N<sub>4</sub>@Ag/BiVO<sub>4</sub> (040) with enhanced visible-light-induced photocatalytic oxidation performance, *Appl. Catal. B: Environ.* 221 (2018) 97–107.
- [64] T.Y. Ma, Y.H. Tang, S. Dai, S.Z. Qiao, Proton-functionalized two-dimensional graphitic carbon nitride nanosheet: an excellent metal-/label-free biosensing platform, *Small* 10 (2014) 2382–2389.
- [65] L. Lu, B. Wang, S.M. Wang, Z. Shi, S.C. Yan, Z.G. Zou, La<sub>2</sub>O<sub>3</sub>-modified LaTiO<sub>2</sub>N photocatalyst with spatially separated active sites achieving enhanced CO<sub>2</sub> reduction, *Adv. Funct. Mater.* 27 (2017) 1702447.
- [66] P. Niu, L.C. Yin, Y.Q. Yang, G. Liu, H.M. Cheng, Increasing the visible light absorption of graphitic carbon nitride (melon) photocatalysts by homogeneous self-modification with nitrogen vacancies, *Adv. Mater.* 26 (2014) 8046–8052.
- [67] P.J. Yang, H.H. Ou, Y.X. Fang, X.C. Wang, A facile steam reforming strategy to delaminate layered carbon nitride semiconductors for photoredox catalysis, *Angew. Chem. Int. Ed.* 56 (2017) 3992–3996.
- [68] J.S. Zhang, M.W. Zhang, C. Yang, X.C. Wang, Nanospherical carbon nitride frameworks with sharp edges accelerating charge collection and separation at a soft photocatalytic interface, *Adv. Mater.* 26 (2014) 4121–4126.
- [69] G. Zhang, Q.H. Ji, Z. Wu, G.C. Wang, H.J. Liu, J.H. Qu, J.H. Li, Facile “spot-heating” synthesis of carbon dots/graphitic carbon nitride for solar hydrogen evolution synchronously with contaminant decomposition, *Adv. Funct. Mater.* 28 (2018) 1706462.
- [70] X.C. Gao, J. Feng, D.W. Su, Y.C. M., G.X. Wang, H.Y. Ma, J.T. Zhang, In-situ exfoliation of porous carbon nitride nanosheets for enhanced hydrogen evolution, *Nano Energy* 59 (2019) 598–609.